Journal of Machine Engineering, 2026, Vol. 26
ISSN 1895-7595 (Print) ISSN 2391-8071 (Online)

Received: *12 March 2026* /Accepted: *19 May 2026* / Published online: *02 June 2026*

restrike operation,
stamping,
spring back,
AutoForm

Mohamed BOUZAFFOUR[1*],
Mohammed NASSRAOUI[1],
Otmane BOUKSOUR[1]

RESTRIKE FORMING OPTIMIZATION FOR IMPROVED GEOMETRY AND REDUCED THINNING

The restrike operation is very important for keeping the shape and quality of stamped parts stable. This study looks at how restrike helps in the stamping process by fixing issues like spring back and surface quality. The first part of the study shows why restrike is needed to prevent problems such as cracks or too much thinning that can happen when making certain parts. This was done using simulations on an outer reinforcement with Auto Form. The second part shows how restrike helps improve spring back. Two simulations were done on different parts using Auto Form: the side member and the rear wheel arch. An experiment was also carried out to support the findings. The results show that restrike greatly reduces spring back and helps fix thinning and cracking problems.

1. INTRODUCTION

Geometric accuracy is a critical requirement in the automotive industry, particularly in the stamping of body-in-white components, which represents a key stage in the assembly process. However, springback caused by the elastic recovery of the material after unloading remains one of the major challenges in sheet metal stamping. This phenomenon leads to significant deviations from the nominal geometry [1, 2], complicating part assembly at the body-in-white stage and potentially increasing costs due to tooling modifications.

Among the earliest studies into springback reduction, significant focus was placed on bead and step-bead techniques. In a comparative study, M. Bouzaffour et al. [3] showed that the step-bead approach offers more effective springback control, leading to enhanced geometric accuracy of stamped parts.

The blank's geometry has a direct impact on springback behavior. Based on simulation tests, a blank with a sinusoidal form improves springback control and provides a final

[1] Laboratory of Mechanics, Production and Industrial Engineering, LMPGI, Higher School of Technology of Casablanca, Morocco
[*] E-mail: mohamed.bouzaffou-etu@etu.univh2c.ma
https://doi.org/10.36897/jme/222225

geometry which is more precise [4]. Also, the holes in the blank are important because they change how stresses and strains are distributed during forming, which impacts the rate of springback [5]. Regarding the characteristics of the blank, the sheet thickness can also affect springback, as other research [6, 7] has shown. According to their findings, springback decreases with increasing sheet thickness, which is advantageous for achieving better geometric accuracy.

One of the critical factors in controlling springback during hot stamping is the cooling rate. By properly managing this rate, it is possible to significantly reduce or even completely eliminate springback, thanks to improved regulation of metallurgical transformations and residual stress distribution within the part [8].

Compared to a bare sheet, the presence of a galvanized coating intensifies the springback effect. This effect becomes more pronounced as the zinc coating thickness increases, as it not only alters the distribution of residual stresses but also impacts the overall behavior of the sheet during the release of forming forces [9].

It has been demonstrated that high-speed bending (IHB, or Impact Hydroforming Bending, depending on the situation) can significantly decrease the springback of Ti-6Al-4V in bending processes. This phenomenon is explained by the high strain rate, which affects how internal stresses are distributed and reduces elastic recovery after forming, improving the part's geometric accuracy [10].

Tool compensation involves modifying the geometry of stamping dies to account for the part’s springback after forming [11]. This adjustment enables the final part to more accurately achieve its intended dimensions and shape, as springback can be partially or completely compensated. Moreover, by allowing the stamping tools to be adapted to local variations in deformation, this approach improves both the geometry accuracy and overall quality of the stamped part [12].

Restrike is another important process that builds on the previously studied factors and has a strong effect on the springback of stamped parts [13]. Recent studies on coining have shown that when applied after deep drawing, this process can noticeably change the final shape of the parts. However, its effectiveness depends greatly on how it is performed: a correctly positioned and controlled restrike can help reduce springback, while a poorly applied one may increase elastic recovery, mainly due to unwanted geometric effects and material flow [14].

A key method for controlling springback and achieving high geometric quality in stamped parts is the restrike process. Including restrike in the tooling design allows localized plastic deformation to be applied to critical areas of the part. This targeted deformation increases the rigidity of the formed areas and reduces springback, greatly improving geometric accuracy. Experimental tests have confirmed the effectiveness of this approach, and numerical simulations have proven reliable, providing a strong foundation for guiding actual industrial production [15].

This article looks at the effect of restrike on reducing springback when forming parts using single-action mechanical presses. It explains how this extra step helps correct and stabilize the final shape of the parts after the first forming stage. In addition, the role of restrike in managing localized thinning caused by the initial forming operation is discussed in detail.

2. ELASTOPLASTIC MODELING AND HARDENING LAWS APPLIED TO SPRINGBACK

One of the main scientific and technical challenges in controlling the geometric accuracy of stamped parts is springback, which occurs due to the recovery of the elastic portion of the deformation accumulated during forming. To predict this phenomenon reliably, it is necessary to have an accurate description of the material's elastoplastic behavior, clearly including hardening laws and plasticity rules in the constitutive models used in numerical simulations.

2.1. PLASTIC CONSTITUTIVE LAW

When the stress reaches a certain limit, the material leaves the elastic range and enters an irreversible plastic state. The boundary between these two states is defined by a plasticity criterion, based on a scalar yield function that depends on the stress.

For isotropic metals, criteria such as von Mises and Tresca are often used because they explain the observed plastic behavior well.

Von Mises Yield Criterion

The equivalent stress associated with the Von Mises criterion [16] is defined as :

$$\bar{\sigma}_{vM} = \sqrt{\frac{3}{2} S_{ij} S_{ij}} \tag{1}$$

Where the deviatoric stress tensor is given by :

$$S_{ij} = \sigma_{ij} - \frac{1}{3}\sigma_{kk}\delta_{ij} \tag{2}$$

This definition leads to the following expression :

$$\bar{\sigma}^2_{vM} = \frac{3}{2}\sigma_{ij}\sigma_{ij} - \frac{1}{2}\sigma^2_{kk} \tag{3}$$

Where σ_{ij} are the components of the Cauchy stress tensor, δ_{ij} is the Kronecker delta , and σ_{kk} is the trace of the stress tensor.

And, for a general three-dimensional (triaxial) stress state :

$$\bar{\sigma}^2_{vM} = \frac{1}{2}\left[(\sigma_{11}-\sigma_{22})^2+(\sigma_{22}-\sigma_{33})^2+(\sigma_{33}-\sigma_{11})^2\right]+3(\sigma^2_{12}+\sigma^2_{13}+\sigma^2_{23}) \tag{4}$$

Since the stress tensor is symmetric, it can be diagonalized. In the principal stress basis σ_I, σ_{II} and σ_{III}, the Von Mises equivalent stress is expressed as :

$$\bar{\sigma}^2_{vM} = \frac{1}{2}\left[(\sigma_I-\sigma_{II})^2+(\sigma_{II}-\sigma_{III})^2+(\sigma_{III}-\sigma_I)^2\right] \tag{5}$$

Tresca yield criterion

The Tresca yield condition is predicated on the principle of maximum shear stress [17] results in the subsequent characterization of the equivalent stress:

$$\bar{\sigma}_T = \sup\left(|\sigma_I - \sigma_{II}|, |\sigma_{II} - \sigma_{III}|, |\sigma_I - \sigma_{III}| \right) \quad (7)$$

According to the plasticity conditions and the yield surface, the onset of plasticity is characterized by the satisfaction of the following condition:

$$\bar{\sigma} - \sigma_0 = 0 \quad (7)$$

This equation defines the yield surface in stress space. Stress states located inside this surface correspond to purely elastic behavior, whereas crossing it marks the activation of plasticity. The position and shape of the yield surface are crucial for predicting elastic springback, since it depends on the amount of elastic energy stored during forming and released upon unloading.

2.1. HARDENING LAWS

Hardening laws extend the plastic constitutive framework by describing how the material resistance evolves with increasing accumulated plastic deformation, while incorporating the effects of prior loading on the mechanical response. These laws are typically calibrated using uniaxial tensile tests conducted on standardized specimens [18].

For low tensile loading rates, an extensometer fixed on the gauge section of the specimen is used to measure its elongation during the test [18]. as shown in Fig. 1. This device makes it possible to determine the conventional (engineering) curve of the tensile test, up to fracture. The initial length is denoted L_0,, and the current length L. The maximum elongation is limited to about 15%. At this stage of the test, the extensometer is removed from the gauge section. The conventional stress–strain curve is therefore derived, relating engineering stress to engineering strain. Both quantities are calculated from the measured tensile force F and the elongation $L\text{-}L_0$:

$$\varepsilon_{conv} = \frac{L\text{-}L_0}{L_0} \leq 0{,}15 \text{ and } \sigma_{conv} = \frac{F}{S_0} \quad (8)$$

Where $S_0 = l_0 \times e_0$ represents the initial cross-sectional area of the specimen.

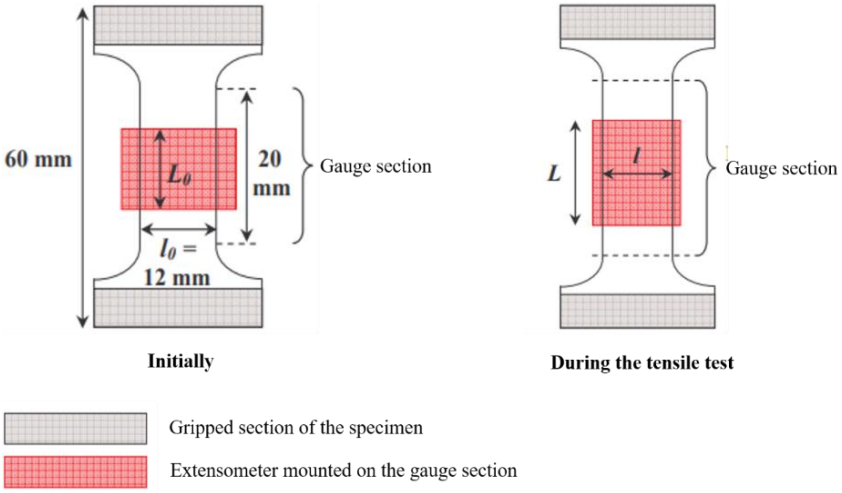

Fig. 1. Geometry of the machined tensile test specimen with thickness e

By using an extensometer, these conventional measurements allow the stress–strain curve to be recorded up to failure, as shown in Fig. 2.

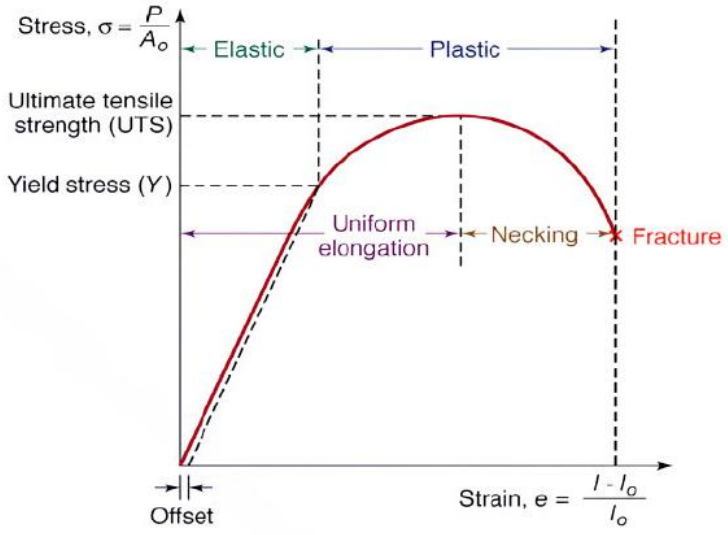

Fig. 2. Conventional stress–strain curve obtained during a tensile test

In a tensile test, the quantities commonly used are the so-called engineering (or conventional) stress and strain, which are calculated based on the initial cross-sectional area S_0 and the initial gauge length L_0, This approach is adequate for small deformations but becomes less representative of the actual material behavior as deformation increases.

Indeed, during the test, the specimen elongates while its cross-sectional area continuously decreases. Engineering quantities (or conventional) do not account for this geometric evolution, since they are defined using the initial dimensions. It is therefore necessary to introduce true stress and strain, which describe the instantaneous state of the material.

The true strain is defined as the sum of incremental elongations relative to the current length, leading to a logarithmic expression:

$$\varepsilon_{true} = \ln(1+\varepsilon_{conv}) \tag{9}$$

Similarly, the true stress is defined using the instantaneous cross-sectional area of the specimen. Assuming plastic incompressibility of the material, the following relationship is obtained :

$$\sigma_{true} = \sigma_{conv}(1+\varepsilon_{conv}) \tag{10}$$

The resulting true stress–true strain curve allows the determination of the material's work-hardening behavior, which describes the evolution of stress as a function of plastic Strain. However, the true strain ε_{true} obtained from the previous relations includes both elastic and plastic contributions. For the purpose of characterizing plasticity, it is therefore necessary to isolate the plastic component of deformation. The total true strain can be decomposed into an elastic part and a plastic part as follows:

$$\varepsilon_{true} = \varepsilon_p + \varepsilon_e \tag{11}$$

The elastic strain ε_e is assumed to follow Hooke's law, using the instantaneous stress and the Young's modulus E:

$$\varepsilon_e = \frac{\sigma_{true}}{E} \tag{12}$$

Thus, the plastic strain can be expressed by subtracting the elastic contribution from the total true strain:

$$\varepsilon_p = \varepsilon_{true} - \frac{\sigma_{true}}{E} \tag{13}$$

In practice, at the onset of yielding, the elastic strain reaches its maximum value, which can be approximated by the ratio of the yield strength **Re** to the Young's modulus **E**. Under this assumption, the plastic strain may be estimated as:

$$\varepsilon_p = \varepsilon_{true} - \frac{Re}{E} \tag{14}$$

Where E is the Young's modulus, Re is the yield strength, ε_{true} is the true strain.

This transformation is essential because work-hardening laws are expressed as a function of plastic strain rather than total strain. Based on the experimental true stress–true strain curve, different hardening laws can then be identified and used in numerical modeling.

At low strain rates, the elastoplastic behavior of metallic materials is commonly described using empirical hardening laws that relate the true stress to the true plastic strain. These constitutive relations capture the progressive increase in material resistance during irreversible deformation.

In these formulations, σ denotes the true stress and ε_p the plastic strain. The parameter K is the strength coefficient, representing the overall stress level of the material, while n is the strain hardening exponent, which governs the sensitivity of the stress evolution with plastic deformation. A higher value of n indicates a stronger hardening response.

The Hollomon law is the simplest power-law representation:

$$\sigma = K\, \varepsilon_p^n \tag{15}$$

the parameter K corresponds to the stress level at a unit plastic strain ($\varepsilon_p = 1$), while n describes the sensitivity of the stress to increasing plastic strain. A higher value of n indicates stronger strain hardening.

The Krupkowski law introduces an additional parameter ε_0:

$$\sigma = K(\varepsilon_p + \varepsilon_0)^n \tag{16}$$

where ε_0 represents a fictitious initial plastic strain. This term improves the fitting of experimental curves, particularly near the yield point, by avoiding zero stress at zero plastic strain.

Finally, the Voce law is written as:

$$\sigma = K(1 - exp\,(-n(\varepsilon_p + \varepsilon_0))) \tag{17}$$

In this case, K represents a saturation stress, towards which the stress tends as plastic strain increases. The parameter n controls the rate of approach to this saturation, while ε_0 adjusts the origin of the plastic strain.

The choice of the hardening law depends on the material response and the required accuracy of the constitutive model. These models are typically calibrated by fitting experimental true stress–true plastic strain curves using regression techniques, allowing accurate identification of the parameters K, n, and ε_0 for numerical simulations.

3. THE ROLE OF RESTRIKE IN MANAGING SPRINGBACK

3.1. STUDIED PARTS AND PROCESS PARAMETERS

Two automotive parts were selected for their geometric complexity and functional requirements. a side member and a wheel arch.

The 2.4 mm-thick side member is formed in three operations (deep drawing, trimming and piercing, and restrike) using a single-action press. It has an open deep draw with a bead around the part as represented in Fig. 3. Its walls expand during forming, generating springback and influencing the assembly with other underbody components.

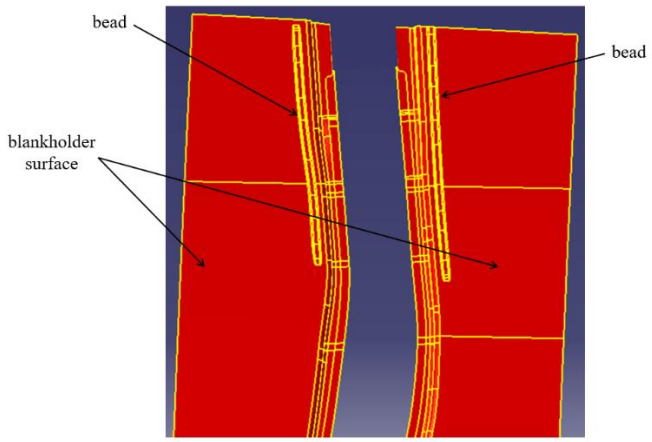

Fig. 3. Forming of the Side Member with a Bead around the Part

The material used is HR380LA, a high-strength steel widely used in automotive structures due to its good mechanical performance and formability.The plastic behavior is modeled in AutoForm using an isotropic Hollomon hardening law. The material parameters are summarized in Table 1.

Table 1. Material properties and anisotropy parameters of HR380LA steel

Property	Symbol	Value
Initial yield stress	σ_0 (MPA)	449.3
Ultimate tensile strength	Rm (MPA)	483.2
Hardening exponent	n	0.0631
r-value (0°)	r_0	0.73
r-value (45°)	r_{45}	1.02
r-value (90°)	r_{90}	0.86

The in-plane anisotropy is described using the Hill 1948 yield criterion, based on the anisotropy coefficients (r_0, r_{45}, r_{90}), allowing an accurate representation of the sheet's directional behavior during stamping.

The second part consists of a 1.2 mm thick wheel arch panel manufactured by a single-action press through three sequential forming stages: deep drawing, trimming and piercing, followed by flanging. As illustrated in Fig. 4, the stamped component represents a single initial blank that results in two distinct wheel arch parts, namely the left wheel arch (yellow areas) and the right wheel arch (orange areas), which are geometrically non-identical due to their asymmetric positions in the vehicle body. A drawbead is implemented along the blankholder surface during the forming stage to control material flow.

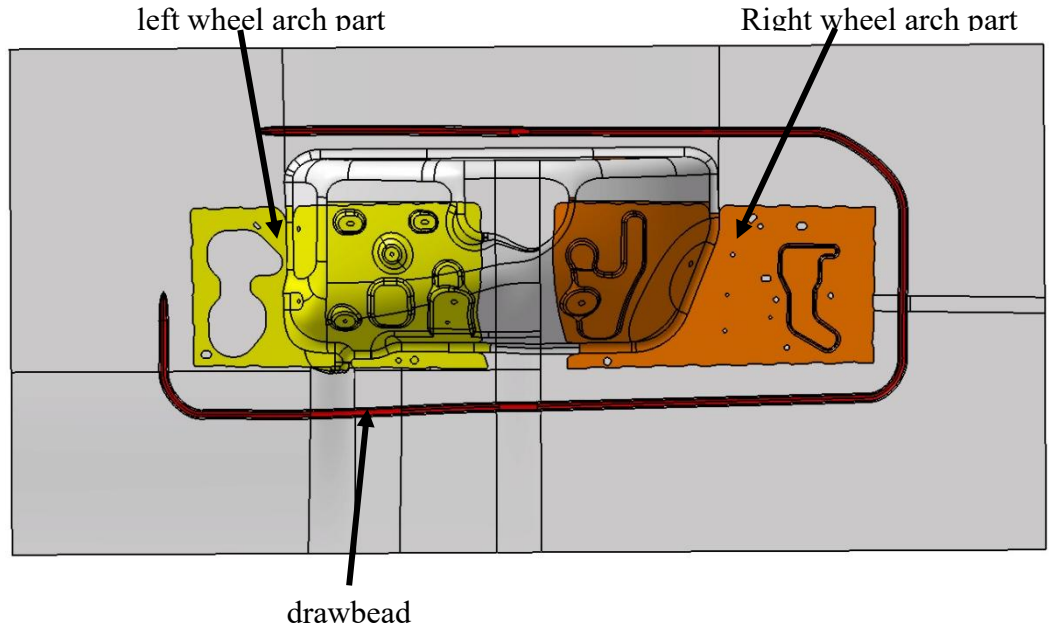

Fig. 4. Forming configuration of the wheel arch

Like the previously analyzed part, this one with the material CR300LA follows the Hollomon hardening law to describe its plastic behavior and uses the Hill's criterion to account for in-plane anisotropy. The anisotropic response is defined through the r-values (r_0, r_{45}, r_{90}). Its complex geometry further increases the difficulty of controlling springback and achieving precise final part geometry. However, this modeling approach allows for a reliable prediction of both stamping behavior and springback effects, the material parameters are summarized in Table 2.

Table 2. Material properties and anisotropy parameters of CR300LA steel

Property	Symbol	Value
Initial yield stress	σ_0 (MPA)	331
Ultimate tensile strength	Rm (MPA)	430.1
Hardening exponent	n	0.105
r-value (0°)	r_0	0.92
r-value (45°)	r_{45}	1.28
r-value (90°)	r_{90}	1.22

3.2. DISCUSSION AND RESULTS

Numerical Simulation Study

To evaluate the springback of the sidemember, an analysis of the springback in AutoForm was performed on the final part after trimming. The results are presented in Fig. 5.

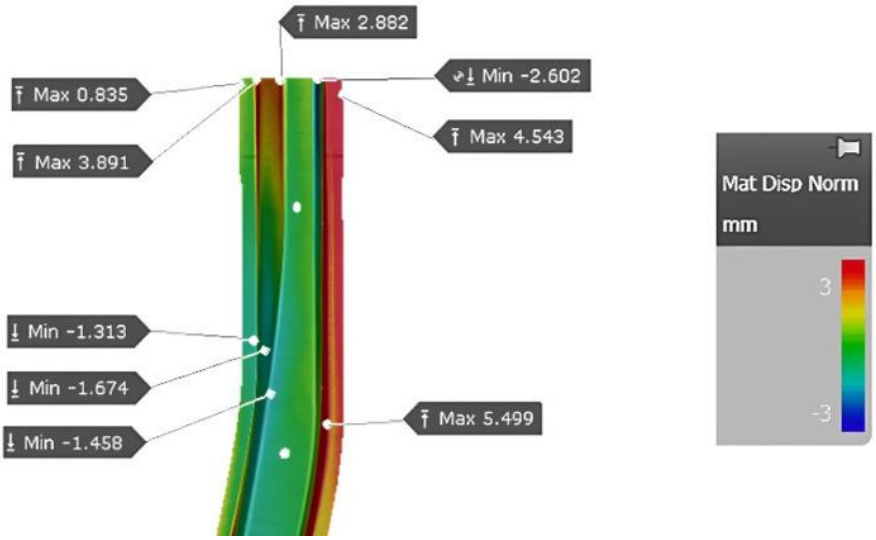

Fig. 5. Springback result of the side member after the final operation

Significant springback is observed, especially in the flange and vertical wall areas, according to the springback results. The results show a significant deviation, measuring between –2.602 mm to +5.499 mm. A test was carried out with a 6 mm wall opening during the first stamping operation, followed by an additional restrike operation to close the walls, as shown in Fig. 6, and the springback result after the restrike operation is presented in Fig. 7.

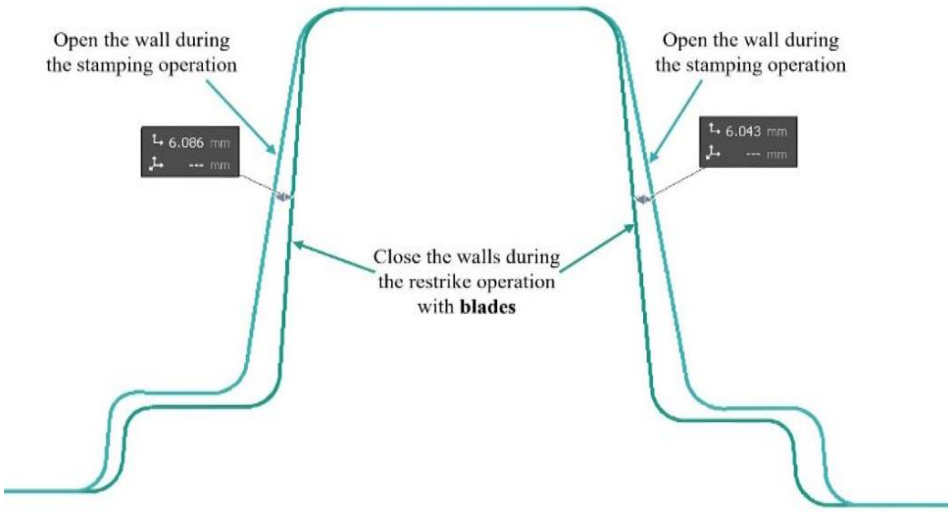

Fig. 6. Wall closing with blade restrike

The areas that initially showed significant springback were effectively corrected by the restrike operation. The deviations are now reduced and measured between −1.009 mm to +1.343 mm, compared to the initial state, where the total deformation amplitude reached 8.101 mm, the restrike reduces it to 2.352 mm, which represents an improvement of approximately 71%, clearly demonstrating its effectiveness in controlling springback and ensuring good geometric conformity.

However, the use of restrike blades induces additional local stresses in the sheet metal. It is therefore necessary to assess their impact on thinning to ensure that no critical areas are affected, the thinning analysis shown in Figure 8 indicates a minimum value of 19.8% for a limit criterion set at 20%. The maximum thinning remains below the limit threshold, confirming that the restrike operation did not exceed the thinning limit.

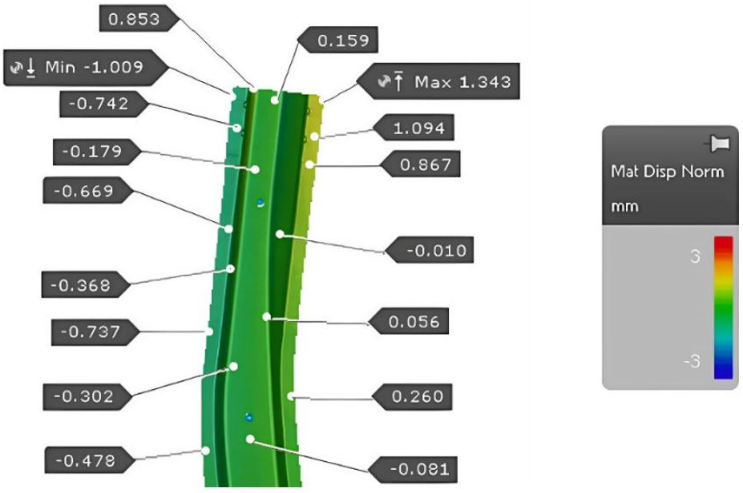

Fig. 7. Springback result of the side member after restrike

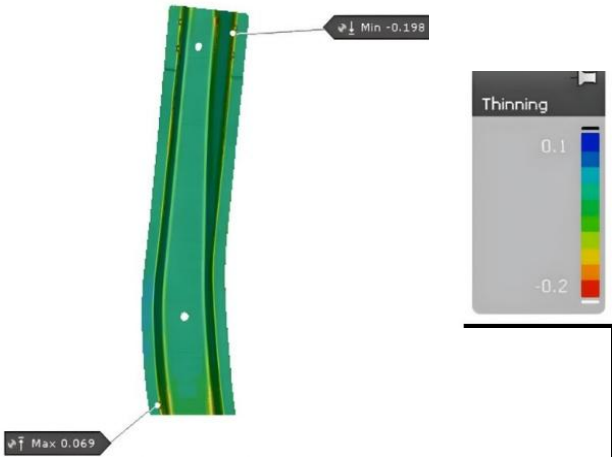

Fig. 8. Thinning results of the side member after the restrike operation with blades

The second part studied is the wheel arch. The springback after trimming the outer contour post-forming is shown in Fig. 9.

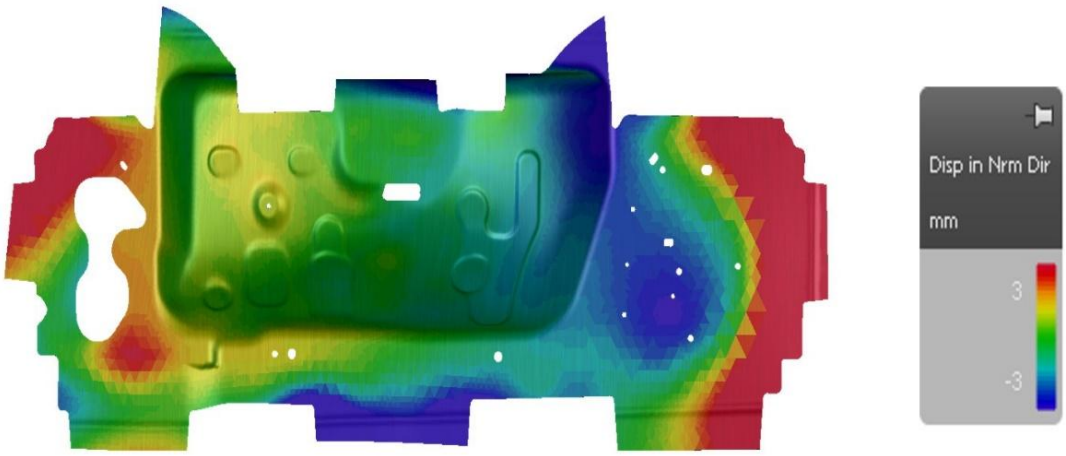

Fig. 9. Springback result of the wheel arch after trimming

Blue and purple areas show inward displacement (up to −3 mm), and red and yellow areas show outward displacement (up to +3 mm), with strong springback on the lateral areas and stability at the center.

A test was done by actuating the pad during the final flange down/up operation to apply a low-amplitude strike on areas with significant springback, aiming to improve the part's final geometry, the pad is shown in Fig. 10, with the yellow areas representing the pad contact surfaces, that is, the areas of the part where the restrike action is. The corresponding springback result is shown in Fig. 11.

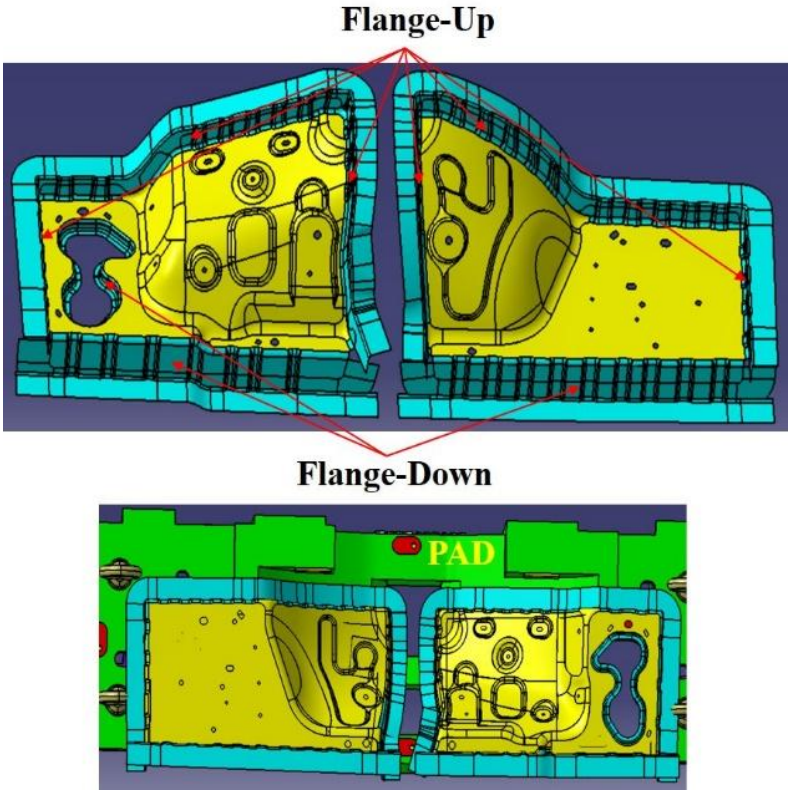

Fig. 10. Illustration of the last operation process and the pad used

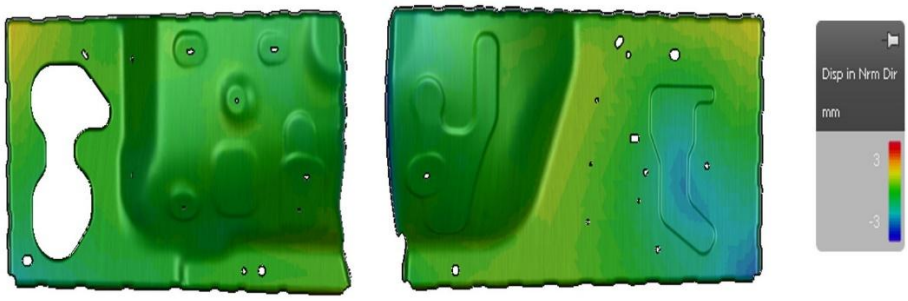

Fig. 11. Springback result of the wheel arch after pad restrike

Most of the part is green, showing near-zero springback. Moderate springback remains in light-yellow areas (+1 mm to +1.5 mm) and a light-blue area (−1.5 mm). Pad restrike reduced residual displacements from ±3 mm to ±1.5 mm, a 50% improvement, effectively enhancing the part's final geometric accuracy, especially in critical zones.

Experimental analysis findings

An experimental test was carried out to quantify the reduction in springback achieved by the proposed method. The dieset incorporated restrike blades, as shown in Fig. 12.

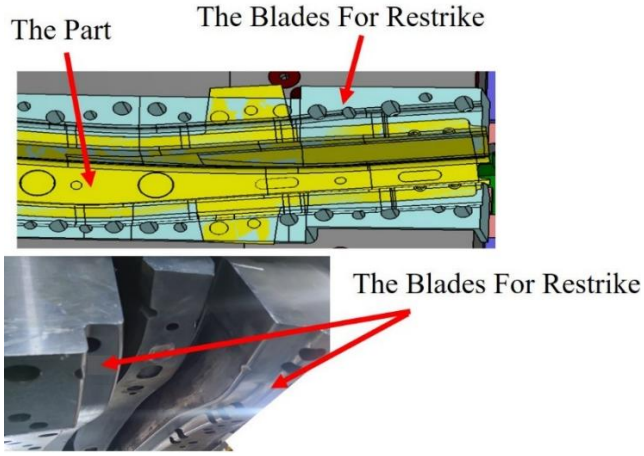

Fig. 12. Representation of the process of the final operation with the implementation of the restrike blades

To validate these results, a forming test was performed with the designed tool. The produced part shown in Fig. 13 was measured using a Coordinate Measuring Machine and compared with the CAD model, as shown in Fig. 14.

Fig. 13. Part produced with the final tool

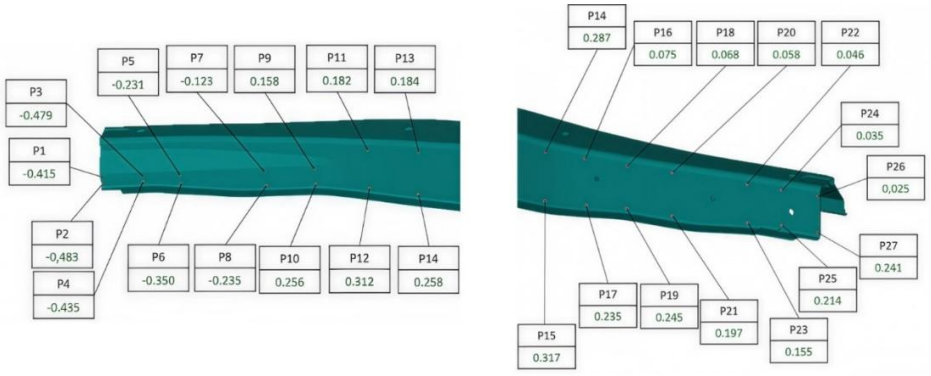

Fig. 14. Measurements points of the part produced

A statistical analysis of the geometric deviations after restrike with blades was performed using control points on the side member, as shown in Table 3. The deviation is calculated as:

$$\sigma = \sqrt{\frac{\sum_{i=1}^{N} (\Delta_i - \mu)^2}{N-1}} \tag{18}$$

Where μ is the mean, and Δ_i is the measured deviation at point i. This indicator indicates how well restrike reduces springback and quantifies geometric dispersion. The side member's statistics results are shown in Table 4.

Table 3. Measurement points

Points	Deviation Δ (mm)
P1	-0.415
P2	-0.483
P3	-0.479
P4	-0.435
P5	-0.231
P6	-0.35
P7	-0.123
P8	-0.235
P9	0.158
P10	0.256
P11	0.182
P12	0.312
P13	0.184
P14	0.258
P15	0.317
P16	0.075
P17	0.235
P18	0.068
P19	0.245
P20	0.058
P21	0.197
P22	0.046
P23	0.155
P24	0.035
P25	0.214
P26	0.025
P27	0.241

Table 4. Statistical analysis results

Number of the points N	μ	σ (mm)	Minimum value (mm)	Maximum value (mm)	Compliance Rate (%)
27	0.01	0.26	-0.483	0.317	100%

The restrike with blades shifts the geometric deviations around the nominal geometry, with a mean value close to zero and a dispersion of about 0.26 mm. Deviations range from −0.48 mm to +0.32 mm, all within the ±1 mm tolerance, confirming geometric conformity. Since $\sigma < T/6 \approx 0.33$ mm, the process is highly stable. Restrike with blades effectively compensates the springback and ensures dimensional conformity across all functional areas, in good agreement with numerical simulation results.

Experimental validation of the wheel arch was performed. After trimming, significant springback was observed in several areas, marked by red contours in Fig. 15. One zone shows particularly pronounced springback, reflecting strong stress relaxation after trimming, in agreement with numerical simulation results. To correct the strong springback observed in critical areas during trimming, a test was performed by actuating the pad during the final flange down/up operation to apply a low-amplitude strike on zones with significant springback, as shown in the previous numerical results (Fig.11). Figure 16 shows the results on the left part after its integration.

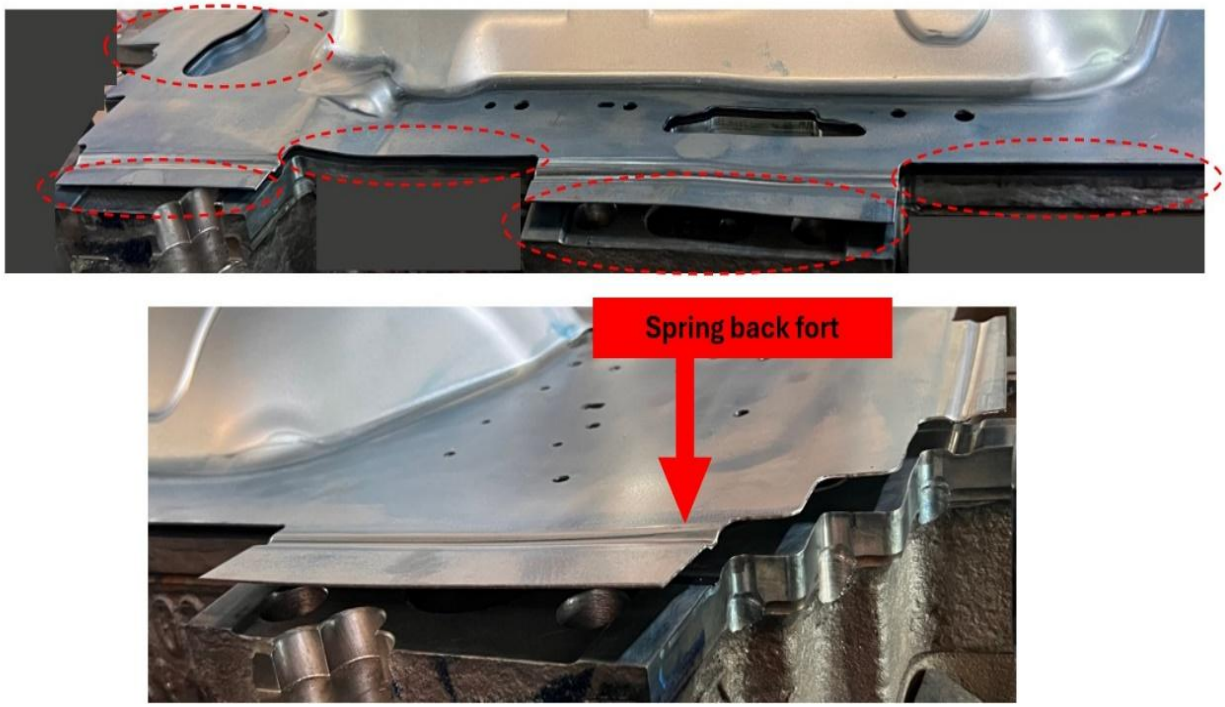

Fig. 15. Areas of spring back observed after trimming the part

Statistical processing of the post-restrike geometric deviations was conducted using the control points given in Table 5, and the results obtained for the left wheel arch are provided in Table 6.

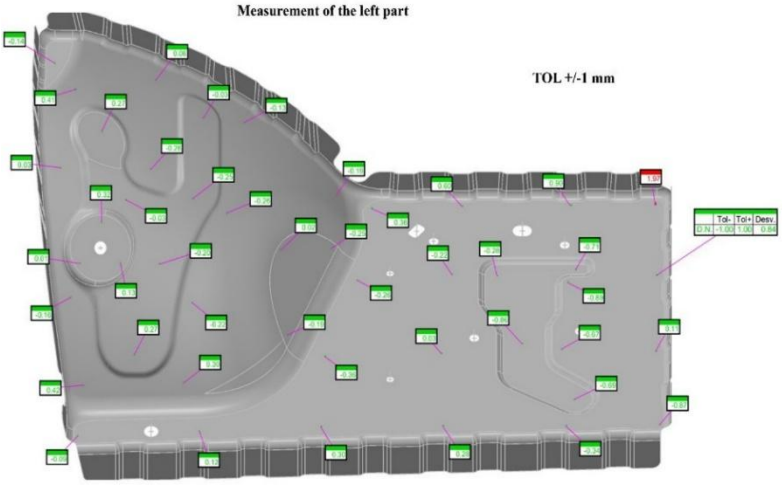

Fig. 16. Measurements points of the left part produced

Table 5. Measurement points

Points	Deviation Δ (mm)
P1	-0.14
P2	0.41
P3	0.27
P4	-0.26
P5	-0.25
P6	-0.03
P7	-0.13
P8	-0.19
P9	0.6
P10	0.9
P11	1.97
P12	0.36
P13	-0.22
P14	-0.28
P15	-0.71
P16	-0.89
P17	-0.67
P18	-0.69
P19	-0.87
P20	0.11
P21	0.28
P22	0.34
P23	0.3
P24	0.12
P25	-0.09
P26	0.42
P27	0.01
P28	-0.16
P29	0.13
P30	-0.2
P31	-0.22
P32	-0.19
P33	-0.36
P34	0.02

Table 6. Statistical analysis results

Number of the points N	μ	σ (mm)	Minimum value (mm)	Maximum value (mm)	Compliance Rate (%)
34	0.05	0.46	-0.89	1.97	97.10%

The statistical analysis of geometric deviations after pad restrike, performed on the left wheel arch, shows limited dispersion, a mean value around 0.05 mm and a dispersion corresponding to 0.46 mm. More than 97% of the measured points meet the ±1 mm tolerance, indicating an overall stable process.

The maximum deviation of +1.97 mm is the only out-of-tolerance point. This localized exceedance is attributed to partial pad contact in that area, leading to insufficient pad contact**.** Improving the contact to ensure full pad contact in this area would bring the deviation within tolerance and ensure full part conformity. Figure 17 presents the results for the right wheel arch after integration of the pad.

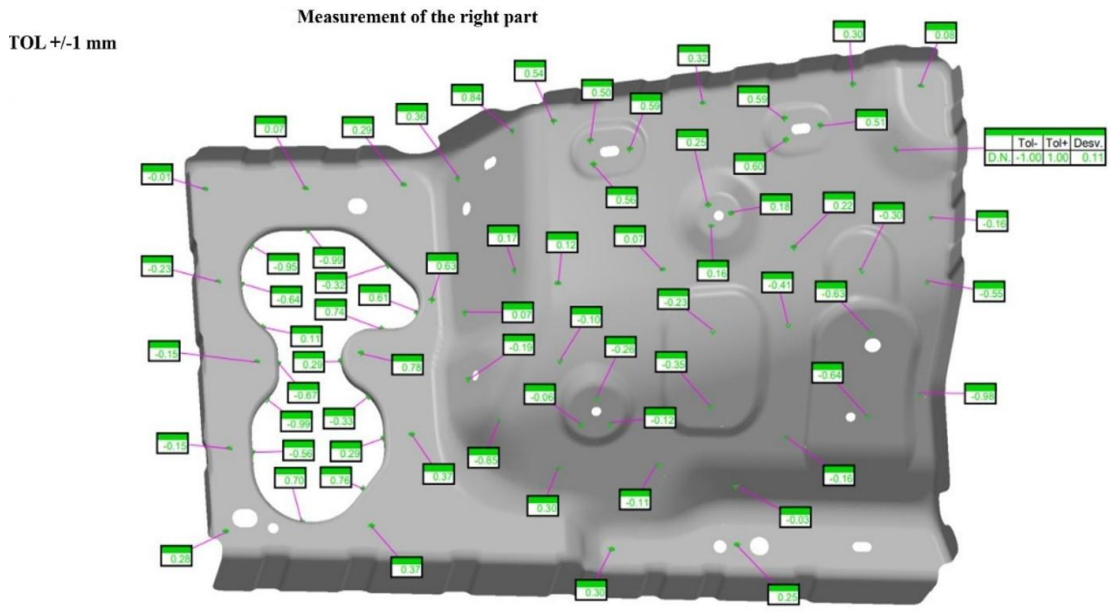

Fig. 17. Measurements points of the right part produced

The measurement points and the statistical analysis results are presented in Tables 7 and 8, respectively.

The statistical analysis of geometric deviations measured on the right wheel arch after pad restrike indicates a distribution centered around the nominal geometry. The average deviation is 0.11 mm, while the standard deviation is 0.44 mm. All measured points meet the ±1 mm tolerance (100% conformity), indicating excellent dimensional control and low geometric dispersion.

Overall, the analysis confirms the effectiveness of pad restrike in stabilizing both right and left wheel arches and in reducing springback, with experimental results in very good agreement with numerical predictions.

Table 7. Measurement points

Points	Deviation Δ (mm)
P1	-0.01
P2	0.07
P3	0.29
P4	0.36
P5	0.84
P6	0.54
P7	0.5
P8	0.59
P9	0.32
P10	0.59
P11	0.6
P12	0.25
P13	0.51
P14	0.3
P15	0.08
P16	0.18
P17	0.22
P18	-0.3
P19	-0.16
P20	-0.55
P21	-0.41
P22	-0.63
P23	-0.64
P24	-0.98
P25	-0.16
P26	-0.03
P27	0.25
P28	0.3
P29	-0.11
P30	-0.12
P31	-0.35
P32	-0.26
P33	-0.1
P34	0.07
P35	0.12
P36	0.17
P37	-0.19
P38	-0.06
P39	0.23
P40	0.16

Table 8. Statistical analysis results

Number of the points N	μ	σ (mm)	Minimum value (mm)	Maximum value (mm)	Compliance Rate (%)
34	0.05	0.46	-0.89	1.97	97.10%

4. CONTRIBUTION OF RESTRIKE TO DEFECT PREVENTION AND SMALL RADIUS FORMING

4.1. STUDIED PARTS AND PROCESS PARAMETERS

In this study, an outer reinforcement was formed using a single-action press in three steps: drawing, trimming and punching, and restrike, as shown in Fig. 18.

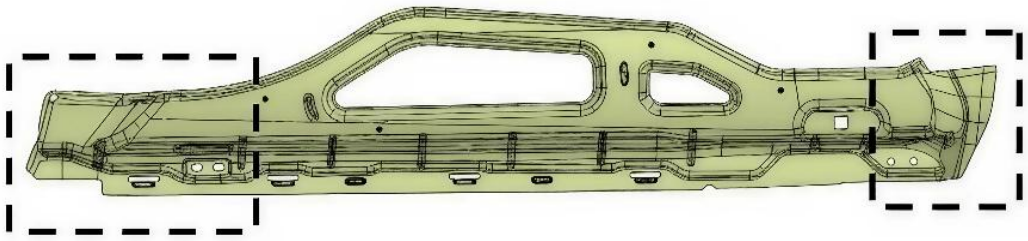

Fig. 18. Outer reinforcement

The following table presents the data:

Table 9. Outer reinforcement Data

Type of Material	Thickness (mm)	Young'modulus(MPA)	Poisson's ratio	Number of operations
E335D	0.8	210000	0.3	3

4.2. DISCUSSION AND RESULTS

Numerical Simulation Study

Figure 19 presents the formability results of the stamped blank prior to the trimming operation. During the stamping process, two symmetric outer reinforcement part (left and right part) are formed simultaneously from the same blank. The final parts shown in Figure 18 are subsequently obtained after trimming. To clarify this relationship, the contours of the final components have been superimposed on the forming results: the black dashed line indicates the left outer reinforcement, while the yellow dashed line corresponds to the right outer reinforcement.

This representation makes it possible to directly assess the formability in the areas associated with each final part. An initial formability assessment was conducted using AutoForm, with the computed results illustrated in Fig. 19.

The risk of crack has been identified in area 1 at the radius, where the material may crack during forming. The section view (A–A) clearly shows this risk. To reduce this issue, the forming process was modified. In operation OP20, the part was formed with a larger radius (R15 mm), which lowers stress and strain concentrations. This improves deformation distribution, enhances formability, and results in a part without defects, as shown in Fig. 20.

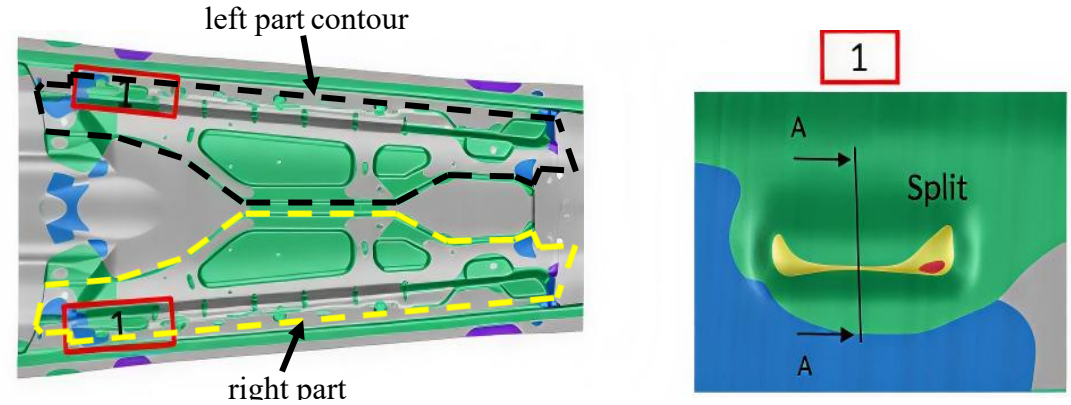

Fig. 19. Outer reinforcement formability

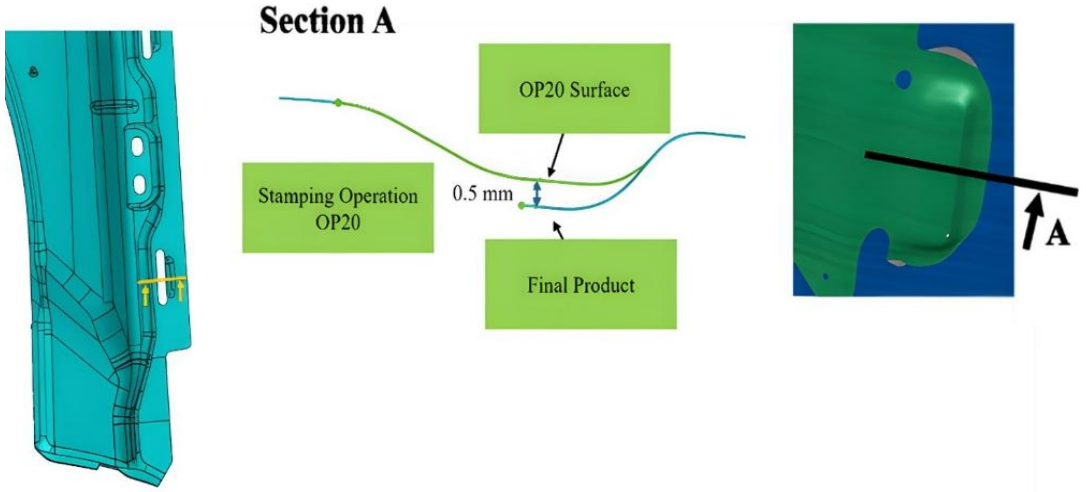

Fig. 20. Intermediate formed part produced during operation OP20 with an enlarged radius (R15 mm)

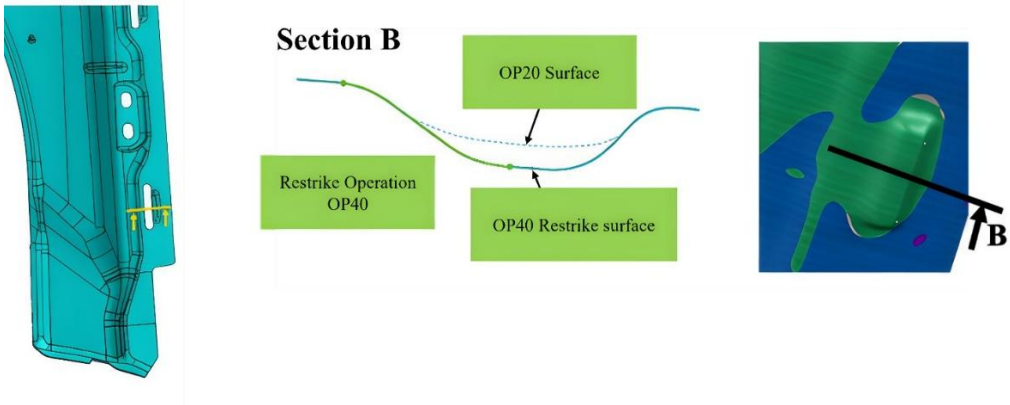

Fig. 21. Restrike operation with radius reduced to R8 mm to achieve the nominal geometry

During the restrike operation OP40, the radius is gradually reduced to R8 to achieve the final geometry, resulting in a safe, defect-free zone (green) in the AutoForm simulation, as shown in Fig. 21:

To prevent the risk of the crack at the radius, the part is formed with a larger radius in OP20 and gradually reduced in OP40, ensuring low stresses and the final geometry.

5. CONCLUSION

This study demonstrates that restrike is essential for optimizing stamped part forming and controlling springback. Numerical simulations with AutoForm, validated experimentally, show that a local restrike significantly reduces springback (about 71% for the side member and 50% for the wheel arch), ensures geometric accuracy, and facilitates assembly. It also limits localized thinning and crack risk, particularly in critical radius areas, by combining initial forming with a larger radius and subsequent restrike. Integrating restrike into the forming process provides a reliable solution for consistent thickness and reduced defects.

However, while the addition of a restrike operation, as in the case of the side member, introduces an additional manufacturing cost related to the extra forming stage, process development (from 3D design through modelling, casting, machining, and procurement of standard components), it significantly improves the quality of the part. In particular, it reduces assembly-related issues such as geometric issues which would otherwise generate additional costs due to extended try-out time during assembly. It also limits iterative tuning efforts in the first stamping operation aimed at correcting geometric deviations, which, in the absence of a restrike operation, typically leads to increased try-out time and higher associated costs. Indeed, attempting to compensate for geometric defects directly during the forming stage is both difficult and time-consuming, often requiring multiple adjustments before achieving acceptable part quality, as well as the risk of part rejection when assembly constraints cannot be satisfied. Consequently, although the restrike operation increases the initial production cost and process complexity, it helps to avoid significant losses related to rework, non-conforming parts, assembly delays, and scrap of geometrically defective parts. In particular, the try-out phase required to correct defects during stamping is very time-consuming, and therefore directly increases production cost.

Similarly, part rejection and scrap also represent a direct financial loss. Overall, restrike improves manufacturing efficiency and process reliability by reducing these time and cost-related issues.

REFERENCES

[1] MA R., WANG C., ZHAI R., ZHAO J., 2019, *An Iterative Compensation Algorithm for Springback Control in Plane Deformation and Its Application*, Chinese J. Mech. Eng., 32/1, https://doi.org/10.1186/s10033-019-0339-5.

[2] REDDY B.L., RAO B.C., REDDY P.R., REDDY P.V.R.R., 2014, *A Review on Springback in Metal Forming*, International Journal of Engineering Research & Technology, 3/1, 646–655.

[3] BOUZAFFOUR M., YASSINE F., NASSRAOUI M., 2025, *Effect of the Choice of Drawbead Type on the Spring Back: Comparative Study Between Two Types of Drawbead*, Int. J. Appl. Mech. Eng., 30/3, 11–25, https://doi.org/10.59441/ijame/205460.

[4] BOUZAFFOUR M., NASSRAOUI M., BOUKSOUR O., 2022, *An Overview of Deep Drawing*, Iste Open sciences, 1–18, https://doi.org/10.21494/ISTE.OP.2023.0920.

[5] SHARAD G., NANDEDKAR V., DHARMALINGAM G., SALUNKHE S., TARIGONDA H., 2023, *Effect of Presence of Holes Locations and Size on Spring Back in U Bent Components*, Mater. Today Proc., https://doi.org/10.1016/j.matpr.2023.02.090.

[6] TEJYAN S., KUMAR N., KANT RAVI R., SINGH V., GANGIL B., 2024, *Analysis of Spring Back Effect for AA6061 Alloy Sheet Using Finite Element Analysis*, Mater. Today Proc., https://doi.org/10.1016/j.matpr.2024.05.122.

[7] KEBDANI O., RADI B., 2021, *Elastic Springback of U-Shaped Stretcher Parts: Study of the Influence of Geometric Parameters on Bottom Twist in Deep Drawing*, Uncertainty and Reliability of Multiphysics Systems, Iste Open sciences, 5/1, https://doi.org/10.21494/iste.op.2021.0716.
[8] SAJAN M., AMIRTHALINGAM M., CHAKKINGAL U., 2021, *A Novel Method for the Spring-Back Analysis of a Hot Stamping Steel*, J. Mater. Res. Technol., 11, 227–234, https://doi.org/10.1016/j.jmrt.2021.01.017.
[9] GUPTA T.R., SIDHU S.S., PAYAL H.S., 2018, *Effect of Die Width on Spring Back of Electrogalvanized CR4 Steel During Air Bending*, Mater. Today Proc., 5/9, 18416–18425, https://doi.org/10.1016/j.matpr.2018.06.182.
[10] Li H., XIE S., ZHANG S., CHEN S., SONG H., XU Y., POKROVSKY A., KHINA B., 2023, *Spring-Back Behaviors of Ti-6Al-4V Sheet Under Effect of Strain Rate*, Int. J. Mech. Sci., 260/April, 108646, https://doi.org/10.1016/j.ijmecsci.2023.108646.
[11] GAVALI S., KULKARNI P.R.R., 2021, *Design and Optimization Process of Press Tools Using Forming Analysis for Frame Bonnet Front Automobile Panel*, Journal of Science & Technology, 06/01, 571–579.
[12] SISWANTO W.A., ANGGONO A.D., OMAR B., JUSOFF K., 2014, *An Alternate Method to Springback Compensation for Sheet Metal Forming*, Sci. World J., https://doi.org/10.1155/2014/301271.
[13] BILLADE B.R., DAHAKE P.S.K., 2018, *Optimization of Forming Process Parameters in Sheet Metal Forming of Reinf-Rr End Upr-Lh / Rh For Safe Thinning*, Journal of Engineering Research and Application, 2248–9622, 8, Part -I, 01-07, https://doi.org/10.9790/9622-0808010107.
[14] GÖSLING M., GÜNER A., BURCHITZ I., THÜLIG T., CARLEER B., 2018, *Effect of Coining on Springback Behaviour*, IOP Conf. Ser. Mater. Sci. Eng., 418/1, https://doi.org/10.1088/1757-899X/418/1/012106.
[15] ZHANG H., WANG T., 2022, *Forming Parameters Multi-Objective Optimization and Mold Design of Vehicle Reinforcement Plate Type Workpieces*, UPB Sci. Bull. Ser. D Mech. Eng., 84/1, 87–102.
[16] MARIGO J., PLASTICITE J.M., 2016, *Plasticity and Fracture*, Springer.
[17] MOHAMED S., 2024, *Concepts of Plasticity*.
[18] LANGE C., 2006, *Physical Study and Numerical Modeling of the Crimping Process of Automotive Body Parts*, HAL Id : pastel-00001760.